PHYSICAL REVIEW C **82**, 044302 (2010)

Prompt and delayed spectroscopy of ^{199}At

U. Jakobsson,[1,*] J. Uusitalo,[1] S. Juutinen,[1] M. Leino,[1] P. Nieminen,[1] K. Andgren,[2] B. Cederwall,[2] P. T. Greenlees,[1] B. Hadinia,[2,†] P. Jones,[1] R. Julin,[1] S. Ketelhut,[1] A. Khaplanov,[2] M. Nyman,[1,‡] P. Peura,[1] P. Rahkila,[1] P. Ruotsalainen,[1] M. Sandzelius,[1] J. Sarén,[1] C. Scholey,[1] and J. Sorri[1]

[1]*Department of Physics, University of Jyväskylä, P.O. Box 35, FI-40014 Jyväskylä, Finland*

[2]*Department of Physics, Royal Institute of Technology, SE-10691 Stockholm, Sweden*

(Received 2 July 2010; published 6 October 2010)

The neutron-deficient nucleus ^{199}At has been studied through γ-ray and electron spectroscopy, using the recoil-decay tagging technique. Two experiments were conducted, using a gas-filled recoil separator with a focal-plane spectrometer alone and together with a germanium-detector array at the target position. The resulting level scheme for ^{199}At includes a new isomer with a half-life of 0.80(5) μs and a spin and parity of $(29/2^+)$. The $13/2^+$ isomer, which de-excites via an $M2$ transition to the $9/2^-$ ground state, was measured to have a half-life of 70(20) ns. Our earlier version of the level scheme for ^{197}At has been updated as well.

DOI: 10.1103/PhysRevC.82.044302 PACS number(s): 23.20.Lv, 23.35.+g, 27.80.+w, 29.30.Kv

I. INTRODUCTION

The neutron-deficient nuclei in the light lead region exhibit a variety of different shapes. These coexisting configurations involve an excitation of one or more pairs of protons across the $Z = 82$ shell gap, interacting with an increasing number of valence neutrons as the $82 \leqslant N \leqslant 126$ shell becomes depleted [1,2]. The low-lying yrast states in even-mass polonium nuclei, for instance, show a transition from spherical structures toward oblate-deformed and onward to prolate-deformed collective bands when approaching the $N = 104$ mid-shell (see, for example, [3,4] and references therein). Similar behavior could be expected in the odd-mass astatine nuclei, as they have only one proton more than their polonium isotones.

The low-lying states of the neutron-deficient astatine nuclei down to $A = 201$ have been found to be dominated by spherical structures [5–10]. However, a recent in-beam γ-ray spectroscopic study, supported with theoretical total Routhian surface (TRS) calculations, showed evidence of shape coexistence in ^{197}At [11]. The $9/2^-$ ground state is predicted to be nearly spherical, with $\beta_2 \approx 0.1$, in agreement with the observed vibrational level pattern. In contrast, the single-proton $13/2^+$ state, known throughout the odd-mass astatine isotopes down to $A = 193$ (excluding ^{195}At), was observed at an excitation energy of 311 keV and predicted to have an oblate deformation with $\beta_2 \approx 0.2$ in ^{197}At. This conclusion is supported by the observation of the beginning of a strongly coupled band built on this state.

Earlier results for ^{199}At are somewhat varying. Męczyński *et al.* [12] presented a strongly coupled rotational band on top of the $9/2^-$ ground state. Styczeń *et al.* [13], however, placed it on top of the $13/2^+$ isomer, which was suggested to have an excitation energy of 466 keV and a half-life of the order of 1 μs. The isomeric decay itself was not detected. In a later study, Lach *et al.* [14] observed a delayed 573-keV γ-ray transition showing a half-life of 580(130) ns. They assigned it as the single-step de-excitation of the $13/2^+$ isomer to the $9/2^-$ ground state.

The present work aims to resolve the discrepancies among the previous results for ^{199}At and to investigate more thoroughly the shape competition in ^{199}At. In addition, an updated level scheme for ^{197}At is presented, based on an independent analysis of the data used in Ref. [11].

II. EXPERIMENTAL DETAILS

The measurements were conducted in the Accelerator Laboratory at the Department of Physics of the University of Jyväskylä (JYFL), Finland. The nucleus ^{199}At was produced in two different fusion-evaporation reactions, ^{150}Sm(^{52}Cr, $p2n$)^{199}At and ^{120}Sn(^{82}Kr, $p2n$)^{199}At, where the main goal was an in-beam study of ^{199}Rn [15]. In the first reaction, the beam of ^{52}Cr, provided by the K-130 cyclotron, was accelerated to an energy of 231 MeV with an average beam current of 17 particle-nA (pnA) (80 h irradiation time). The target consisted of two foils of ^{150}Sm with a total thickness of 500 μg/cm^2. The targets were evaporated on a 10 μg/cm^2 thick carbon backing foil and an additional carbon reset foil, with a thickness of 42 μg/cm^2, was used behind the stacked target. The target material included contamination by small amounts of more abundant heavier samarium isotopes. This resulted in a high population of ^{202}Rn, which has a half-life and α decay energy similar to those of ^{199}At. For the second reaction a beam of ^{82}Kr, with an energy of 355 MeV and an average intensity of 10 pnA (60 h irradiation time), was used to bombard a self-supporting ^{120}Sn target. The target had a thickness of 500 μg/cm^2, and a 42 μg/cm^2 thick carbon reset foil was used. In these two reactions, ^{199}At was populated with cross sections of approximately 10 and 15 μb, respectively.

The JUROGAM Ge-detector array was used to detect prompt γ rays at the target position. The array consisted of 43 Compton-suppressed high-purity germanium (HPGe) detectors of EUROGAM Phase1 [16] and GASP type [17].

*ulrika.jakobsson@jyu.fi

†Current address: Department of Physics, University of Guelph, Guelph, Ontario N1G2W1, Canada.

‡Current address: Laboratory of Radiochemistry, University of Helsinki, P.O. Box 55, FI-00014 Helsinki, Finland.

The recoiling fusion-evaporation products were separated from beam particles and other unwanted reaction products by the gas-filled recoil separator RITU [18] and transported to the GREAT spectrometer [19]. When arriving in GREAT, the recoils passed through a multiwire proportional counter (MWPC) and were finally implanted into a 300-μm-thick double-sided silicon strip detector (DSSD), which has 4800 pixels in total. A planar and a clover germanium detector were used to detect delayed γ rays close to the DSSD, and a silicon PIN detector array, situated upstream from the DSSD, was used for measuring conversion electrons. All data channels were recorded synchronously using the triggerless total data readout (TDR) [20] data acquisition system, which gives each event an absolute time stamp with a time resolution of 10 ns.

An additional third measurement, using only RITU and GREAT, was conducted to improve the quality of the previously obtained focal-plane data. An ^{40}Ar beam, with an energy of 200 MeV, was used to bombard a self-supporting ^{165}Ho target with a thickness of 340 μg/cm^2. A carbon reset foil with a thickness of 70 μg/cm^2 was used behind the target. The nucleus ^{199}At was produced in the 6n fusion-evaporation channel with a cross section of approximately 0.7 mb. Alongside ^{199}At, the polonium isotopes ^{198}Po, ^{199}Po, and ^{200}Po were relatively strongly populated through pxn fusion-evaporation channels. A beam current of 6 pnA was chosen to obtain clean γ-ray spectra, reducing random correlations caused by the contaminating polonium isotopes. A higher beam current of 40 pnA was used to collect γ-γ coincidences. The total irradiation time was 30 h. Two clover HPGe detectors [21] were added to the focal-plane setup alongside the GREAT clover detector for an improved high-energy γ-ray detection efficiency.

The nucleus ^{197}At was produced in a separate experiment. The ^{118}Sn(^{82}Kr, $p2n$)^{197}At reaction was used with a beam energy of 362 MeV and a target thickness of 500 μg/cm^2. A description of the experimental details for the ^{197}At measurement is presented in the work by Andgren *et al.* [11].

III. RESULTS

A. ^{199}At

The data were analyzed using the recoil-decay tagging (RDT) technique [22] and processed using the GRAIN [23] and RADWARE [24,25] software packages. The recoiling fusion-evaporation products were selected by their time of flight between the MWPC and the DSSD and their energy loss in the MWPC. Furthermore, the different isotopes were identified by linking the recoils with their subsequent α decays in the DSSD, using spatial and temporal correlations. The α-decay branch of approximately 90% [26] and half-life of 6.92 s [27] for the $9/2^-$ ground state allowed for an effective identification of the ^{199}At recoils, using a maximum correlation time of 21 s between the detection of a recoil and its subsequent α decay. The α-particle energy spectrum obtained from the ^{82}Kr + ^{120}Sn reaction is shown in Fig. 1. Prompt and delayed γ rays belonging to ^{199}At were identified based on their time correlation with the α-tagged recoil observed in the DSSD. For the prompt γ rays detected in the JUROGAM detector array, this time gate was set by taking into account the flight time of approximately 600 ns of the recoils through RITU.

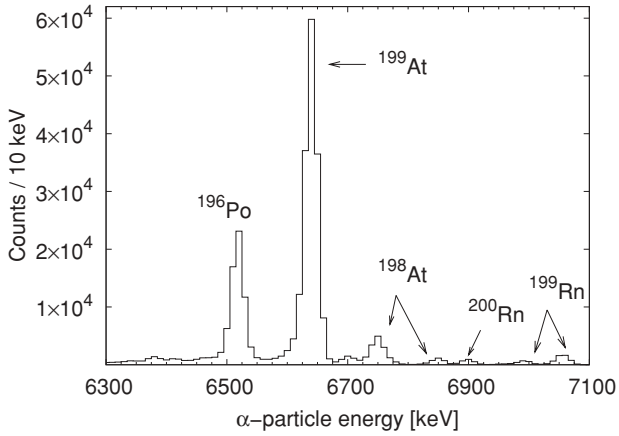

FIG. 1. The α-particle energy spectrum obtained using the ^{82}Kr + ^{120}Sn reaction. A maximum correlation time of 21 s was set between the implantation of the recoil and its subsequent α decay.

The measured prompt data from the ^{150}Sm(^{52}Cr, $p2n$)^{199}At and ^{120}Sn(^{82}Kr, $p2n$)^{199}At reactions were summed to gain statistics for a γ-γ coincidence analysis. A spectrum of prompt γ rays tagged with the α decay of ^{199}At is shown in Fig. 2(a). Figure 2(b) presents the energy spectrum of the coincident γ rays obtained by setting an energy gate on the 600-keV γ-ray peak, which is the strongest γ-ray peak in the spectrum of Fig. 2(a). The gated spectrum confirms the doublet nature of the 600-keV peak, as reported by Styczeń *et al.* [13]. In the present work the 600-keV transitions were placed lowest in a cascade on top of the ground state, according to the high intensity of the doublet peak, at variance with the previous work. By examining γ-γ coincidences, the 559-keV transition was identified to precede this doublet. The 92-keV γ-ray transition reported in Ref. [13] was not observed. The intensity division between the transitions in the 600-keV doublet was made by comparing the intensity

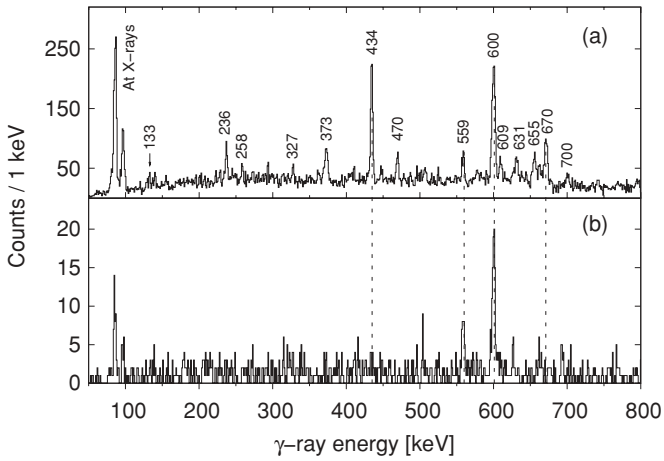

FIG. 2. (a) Spectrum of singles prompt γ rays tagged with the α decay of ^{199}At, collected from the ^{120}Sn(^{82}Kr, $p2n$)^{199}At reaction. (b) Spectrum of γ rays in coincidence with the 600-keV doublet, obtained from the ^{150}Sm(^{52}Cr, $p2n$)^{199}At and ^{120}Sn(^{82}Kr, $p2n$)^{199}At reactions. The dashed lines are inserted to guide the eye for some relevant coincidence-anticoincidence relations.

TABLE I. The γ-ray energies and relative intensities for transitions assigned to ^{199}At.

E_γ (keV)	I_γ (%) delayed	I_γ (%) prompt	I_i^π	I_f^π	E_γ (keV)	I_γ (%) delayed	I_γ (%) prompt	I_i^π	I_f^π
53.8(3)	6(2)	–	$(25/2^+)$	$(23/2^+)$	572.9(1)	100(11)	–	$13/2^+$	$9/2^-$
(70(1))[a]	–	–	$21/2^+$	$21/2^+$	(597.3(6))	15(6)	–	–	–
133.1(5)	16(2)	5(1)	$(23/2^+)$	$21/2^+$	600.0(10)[b]	–	53(3)	$17/2^-$	$13/2^-$
162.9(2)	56(2)	–	$(29/2^+)$	$(25/2^+)$	600.0(10)[b]	–	118(3)	$13/2^-$	$9/2^-$
(187.3(3))	9(2)	–	$(25/2^+)$	$21/2^+$	610.0(3)[c]	18(5)	25(5)	$19/2^+$	$15/2^+$
(202(1))[a]	–	–	$(23/2^+)$	$21/2^+$	631.0(3)	33(7)	28(4)	$21/2^+$	$17/2^+$
236.3(6)	15(3)	16(2)	$17/2^+$	$15/2^+$	655.3(2)	–	39(3)	$(11/2^-)$	$9/2^-$
258.5(3)	10(3)	8(2)	$21/2^+$	$19/2^+$	(662.5(3))	–	24(3)	–	–
327.0(4)	21(5)	10(2)	$21/2^+$	$19/2^+$	670.1(3)[b]	38(6)	61(4)	$17/2^+$	$13/2^+$
372.4(5)	16(5)	31(2)	$19/2^+$	$17/2^+$	670.1(3)[b]	–	–	$(25/2^+)$	$21/2^+$
434.0(2)	44(7)	100(4)	$15/2^+$	$13/2^+$	699.9(3)	49(8)	15(2)	$21/2^+$	$17/2^+$
469.6(2)	–	20(2)	–	$15/2^+$	(795.2(3))	–	14(2)	–	–
558.5(2)	–	28(3)	$21/2^-$	$17/2^-$					

[a]The transition has been tentatively identified (see Fig. 5 and text for details).
[b]The peak is a doublet.
[c]The peak includes events from the 611.2-keV transition in ^{200}Po [28].

of the 600-keV peak in the singles spectrum and the gated spectrum [Fig. 2(b)]. The 655-keV transition [see Fig. 2(a)] was not in coincidence with any strong transition assigned to ^{199}At. It is assumed to depopulate the expected $11/2^-$ state to the ground state. These levels are indicated as the newly assigned Band 1 in the level scheme shown in Fig. 4. The properties of the γ-ray transitions assigned to ^{199}At are listed in Table I.

The delayed γ-ray energy spectra in Fig. 3 are collected from α-tagged events detected in the clover detectors, with a 5-μs correlation time gate. It is evident that several γ-ray transitions (236, 373, 434, 609, and 670 keV) in the singles spectrum of Fig. 2(a) were also detected at the focal plane

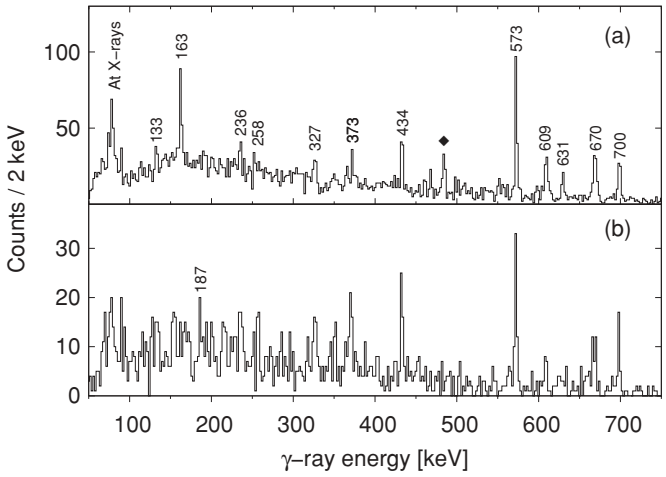

FIG. 3. Delayed γ rays tagged with the ^{199}At α decay, detected in the clover detectors. (a) Spectrum of delayed singles γ rays obtained with lower beam intensity. (b) Spectrum of γ rays in coincidence with the 163-keV transition detected in the planar detector. The 484-keV peak, denoted by a diamond, belongs to ^{200}Po. The data are obtained from the ^{165}Ho(^{40}Ar,6n)^{199}At reaction; a maximum correlation time of 5 μs was set between the recoil and its isomeric decay.

[Fig. 3(a)], indicating the existence of a new high-lying isomer in ^{199}At. These transitions belong to the previously reported level structure [13], placed to feed the expected $13/2^+$ isomer. This study focused on prompt γ-ray spectroscopy, and no high-lying isomer was reported.

Lach *et al.* [14] placed the $13/2^+$ isomer at an excitation energy of 573 keV. At the same time, they noted that the level energies suggested by Styczeń *et al.* [13] have to be revised. In the present work, the 573-keV γ ray is the most intense delayed transition assigned to ^{199}At [see Fig. 3(a)]. Additionally, the 573-keV transition is the only transition that shows two components in the recoil-γ time-difference spectrum. These observations support the assignment made by Lach *et al.* [14]. A 466-keV transition, suggested by Styczeń *et al.* [13], was not observed. Their suggestion that the half-life of the isomer was on the order of a microsecond and that the excitation energy was 466 keV was based on systematics. The properties of the isomeric states in ^{199}At, as well as results from the conversion electron measurements, will be discussed in the following.

The present results, utilizing γ-γ coincidence studies and energy-sum arguments, largely support the previously reported level structure of the $i_{13/2}$ band based on the $13/2^+$ state [13] (Band 2 in Fig. 4). However, γ-γ coincidences support the placement of a previously unknown 631-keV transition to precede the 670-keV transition, establishing a new level at 1874 keV. The relative intensity of the previously reported 700-keV transition is distinctly weaker in Fig. 2(a) than in Fig. 3(a), indicating that it lies closer to the higher lying isomer and is not part of Band 2. Furthermore, a new level at an energy of 2544 keV was tentatively established.

The delayed 133- and 163-keV transitions visible in Fig. 3(a) do not belong to Band 2 and are thus candidates for transitions in the de-excitation path of the indicated higher lying isomer. The energy spectrum of γ rays gated by the 163-keV transition, presented in Fig. 3(b), shows mostly the

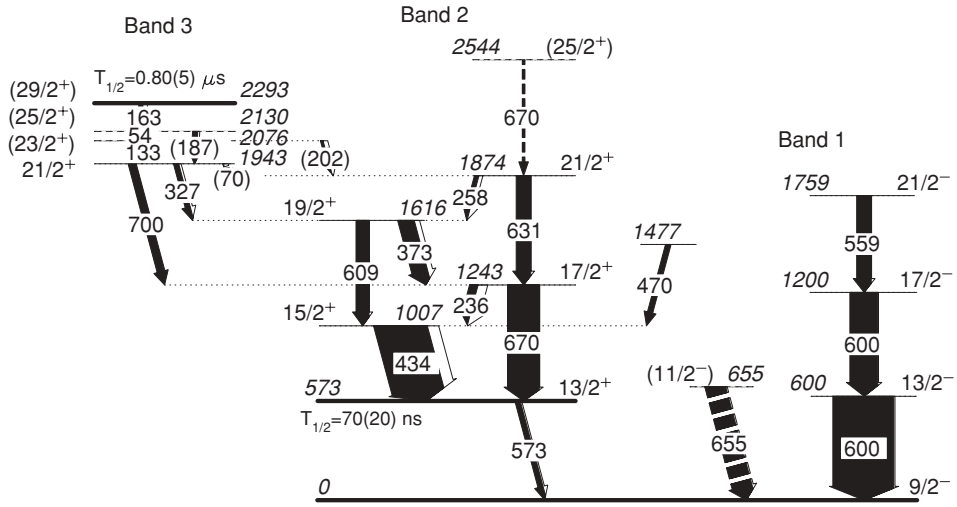

FIG. 4. The proposed level scheme of ^{199}At. The intensities of the 54-, 70-, 133-, 163-, 187-, 202-, and 573-keV transitions below the isomeric states are not to scale.

same transitions as those in Fig. 3(a). Thus, it is likely that the majority of the decay intensity of the isomer proceeds via the 163-keV transition. Although the 163-keV transition is clearly visible in Fig. 3(a) it is not seen in Fig. 2(a), suggesting its placement directly below the isomeric state. In contrast, the 133-keV transition is weakly visible in the α-tagged spectrum of prompt γ rays [Fig. 2(a)], excluding it from being the transitions that depopulates the isomer itself. The suggested de-excitation path of the isomer is shown in the level scheme of Fig. 4, indicated as Band 3.

Figure 5 displays a delayed γ-ray spectrum from the planar detector up to 5 μs after the detection of the ^{199}At recoils. In addition to the 133- and 163-keV transitions, lines at energies of 54, 70, 187, 202, 236, 258, and 327 keV are also observed. The very weak 187-keV transition is in coincidence with the 163-keV transition [see Fig. 3(b)] and, based on

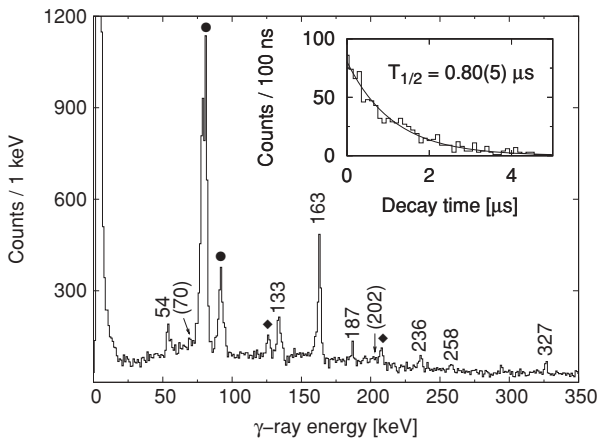

FIG. 5. A spectrum of delayed γ-ray transitions detected in the planar detector within 5 μs after the detection of the ^{199}At recoil in the DSSSD, obtained with lower beam intensity. The inset presents the time distribution between the implantation of a ^{199}At recoil and the observation of the 163-keV γ ray. The filled circles denote the astatine x-ray peaks and the diamonds denote peaks belonging to the polonium isotopes. A spectrum acquired within the time interval of 5–10 μs has been subtracted. The data are obtained from the ^{165}Ho(^{40}Ar,6n)^{199}At reaction.

energy sum arguments, is tentatively placed to proceed in parallel with the 54- and 133-keV transitions. The 631- and 258-keV transitions show weak coincidences with the delayed 163-keV transition [Fig. 3(b)], implying a connection from the high-lying isomer to the $21/2^+$ level at 1874 keV. Weak 70- and 202-keV transitions were tentatively identified (see Fig. 5). They are possibly connecting transitions from states in Band 3 to the $21/2^+$ state in Band 2, allowing the 631- and 258-keV transitions to be detected at the focal plane. Owing to a lack of statistics, the ordering of the transitions in Band 3 remains tentative.

The total internal conversion coefficient of the intense 163-keV transition was estimated by comparing its γ-ray intensity to the total intensity of the 573-keV transition. The resulting value close to 1 indicates an $E2$ multipolarity for the 163-keV transition. By assuming the 133- and 54-keV transitions are in a cascade with the 163-keV transition, with minimal side feeding, an $M1$ multipolarity for both transitions was evaluated. These multipolarities suggest a spin-parity of $29/2^+$ for the isomeric state at 2293 keV. By fitting the time difference between the implantation of the ^{199}At recoil in the DSSD and the detection of the 163-keV transition in the planar detector, a half-life of 0.80(5) μs was determined for the $29/2^+$ isomer (see Fig. 5).

Previously, a half-life of 580(130) ns [14] had been assigned for the $13/2^+$ state. To obtain the half-life of the $13/2^+$ isomer, time differences of transitions in the recoil-gated data below and above the $13/2^+$ state were measured. An energy versus time difference matrix, gated on the 163-keV transition detected in the planar detector, was constructed. The energies of the subsequent transitions, detected in the clover detectors or PIN detector array, were plotted against the time difference with the 163-keV transition. An example of the procedure, using the 474(2)-keV K-conversion electron peak of the 573-keV transition, is shown in Fig. 6. The decay curve was fitted from a point after the drop of the prompt time component. Here the remaining prompt component in the time spectrum originates mainly from the background underneath the peak designated as being due to K conversion. The background component originating from random correlations between the detection of the recoil and the decay event was neglected in

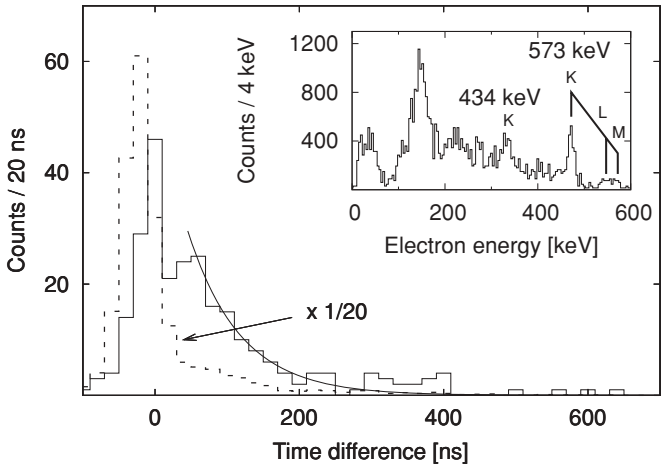

FIG. 6. Time-difference spectrum between the 163-keV γ-ray transition observed in the planar detector and the K-conversion peak of the 573-keV transition observed in the PIN-detector array. The solid line presents the decay curve fitted from 60 ns on. The dashed line, with the intensity compressed by a factor of 20, shows the total projection of the time spectrum for comparison. The inset presents the delayed conversion electron spectrum tagged with the ^{199}At α decay. The K-, L-, and M-conversion peaks of the 573-keV transition are marked in the spectrum together with the K-conversion peak of the 434-keV transition. The data are obtained from the ^{165}Ho(^{40}Ar,6n)^{199}At reaction.

this study. A half-life of 70(20) ns was obtained for the $13/2^+$ state, corresponding to a single-particle transition strength of 0.16(5) W.u. for an $M2$ transition. This result is comparable with corresponding values of an $M2$ transition in neighboring odd-mass astatine nuclei, 0.086(2) W.u. for ^{197}At [11] and 0.182(22) W.u. for ^{201}At [29].

Additionally, a comparison between the 573-keV γ and K-conversion electron peak intensities [in Fig. 3(a) and the inset of Fig. 6] gives a K-conversion coefficient of 0.19(4) for the 573-keV transition, which supports an $M2$ multipolarity as well. The 434-keV $M1$ transition has been used for normalization.

B. ^{197}At

An independent analysis of the ^{197}At data of Andgren *et al.* [11] has been performed, allowing for additional γ-ray transitions to be assigned to the level scheme. The prompt γ-ray spectrum is shown in Fig. 7. The strongly coupled

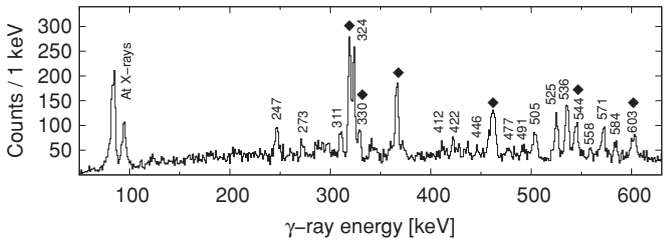

FIG. 7. A prompt γ-ray spectrum tagged with the α decay of ^{197}At, including escaped α particles. Peaks containing events from the contaminating ^{194}Po are denoted with diamonds.

rotational band on top of the $13/2^+$ isomer is extended by two new states with level energies of 1193 and 1796 keV. The latter of these states is denoted as tentative owing to a lack of γ-γ coincidence data.

Some γ-ray transitions evident in Fig. 7 are not associated with the $13/2^+$ isomer, although they clearly belong to ^{197}At. The 505-keV transition is not in coincidence with any of the strong transitions in Band 2 nor with the 536-keV γ-ray transition. It is therefore assigned to depopulate the $11/2^-$ state. The placements of the new 412-, 446-, 477-, and 491-keV γ-ray transitions are based on energy sums and intensity arguments. The extended level scheme for ^{197}At is shown in Fig. 8.

IV. DISCUSSION

Figure 9 presents energy systematics of negative-parity levels in odd-mass astatine and corresponding yrast levels in polonium isotones. The polonium isotopes with $114 \leqslant N \leqslant 124$ have been interpreted to have a vibrational character. Below $N = 114$ the drop in the level energies, particularly visible for the 6^+ and 4^+ states, has been interpreted to be caused by a 2p-2h excitation across the proton shell gap, enhancing the effect of the oblate component in the wave functions [30]. A similar drop, though more gentle for the lower lying states, can be seen for the astatine nuclei in ^{199}At. Because of the resemblance of the energy levels between the corresponding isotones, the states in the astatine nuclei can be interpreted as the odd $h_{9/2}$ proton weakly coupled to the polonium core.

The growing deviation of corresponding states between the isotones around $N = 112$ in Fig. 9 may indicate a strengthening of the coupling between the odd proton and the core. An $11/2^-$ state is assigned tentatively for both ^{197}At and ^{199}At. The energy of this state in ^{199}At is higher than that of the $13/2^-$ state, as can be expected based on the systematics of heavier astatine nuclei (see [5] and references therein). In ^{197}At our candidate for the $11/2^-$ state is below the $13/2^-$ state. This observation further supports the suggestion of a strengthening of the coupling between the mixed configuration of the $h_{9/2}/f_{7/2}$ proton and the polonium core. A similar behavior has been observed earlier in the odd-mass bismuth isotopes (see [33] and references therein). The suggested configuration for each state is shown in Table II.

The excitation energy of the $13/2^+$ state decreases, with decreasing neutron number, and becomes yrast in ^{199}At. A similar decrease for the $13/2^+$ level is seen for example in the odd-mass bismuth isotopes, when approaching the neutron mid-shell. This is interpreted as an effect brought on by a coupling of the $i_{13/2}$ proton to an increasing number of valence neutron holes. This interaction is less repulsive for a proton in the $i_{13/2}$ shell than in the $h_{9/2}$ shell, thus bringing the $13/2^+$ state down in energy [34].

The $13/2^+$ isomer in ^{197}At is interpreted as being oblate deformed [11]. The level spacing in the $i_{13/2}$ band decreases when moving from ^{199}At to ^{197}At. It can also be noted that the signature splitting is larger for ^{199}At in comparison with the corresponding band in ^{197}At. Figure 10 depicts the $B(M1)/B(E2)$ values for the $i_{13/2}$ band of ^{197}At and ^{199}At

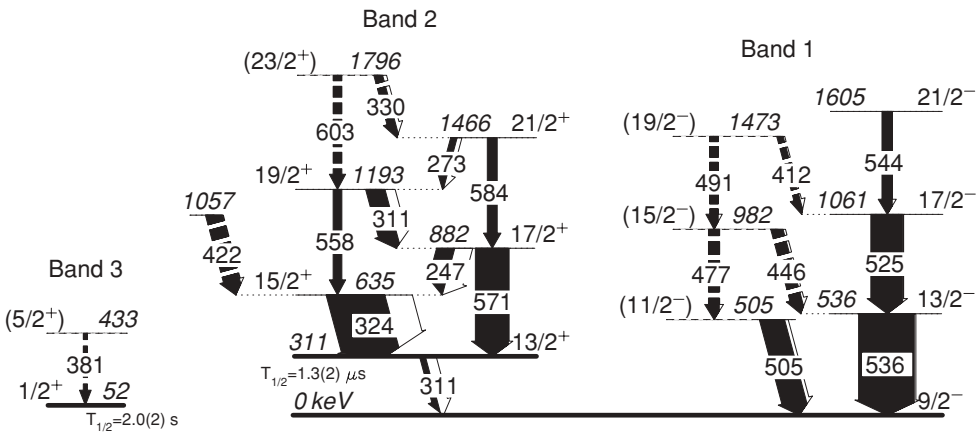

FIG. 8. The level scheme of ^{197}At. The intensity of the isomeric 311-keV transition is not to scale.

compared to the ^{193}Bi nucleus. A theoretical estimate was calculated using the Dönau-Frauendorf model [35,36]. The $B(M1)/B(E2)$ values for ^{199}At are lower than one would expect for a collectively behaving nucleus. This may be caused by a stronger contribution of the spherical components in the wave functions in ^{199}At than in ^{197}At, resulting in a weaker deformation for the states in ^{199}At. The values for ^{197}At and ^{199}At are, nonetheless, of comparable magnitude with those of the $i_{13/2}$ band in ^{193}Bi.

Plots of experimental kinematic moments of inertia $\mathscr{J}^{(1)}$ for the $i_{13/2}$ band in ^{197}At and ^{199}At show similar linear behavior as bands in neighboring oblate deformed nuclei (see Fig. 11). This, together with the observed strongly coupled character of the band, supports the interpretation of oblate structure for the $i_{13/2}$ band in ^{197}At and in ^{199}At.

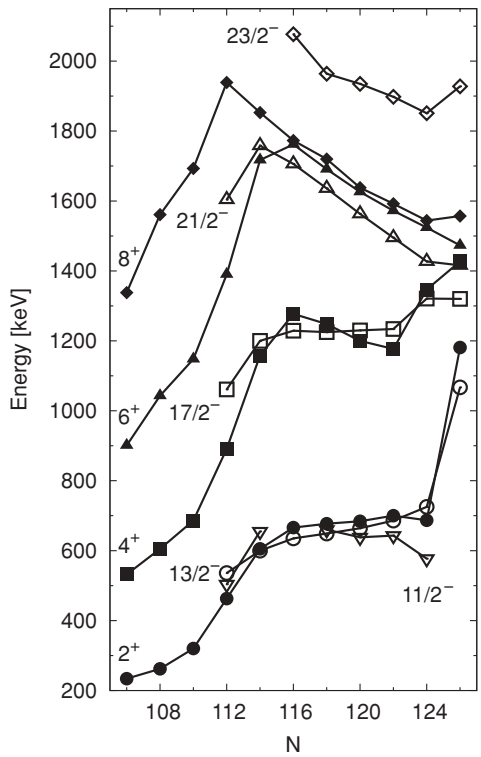

FIG. 9. Level energies of negative-parity states in odd-mass astatine nuclei compared with the yrast states in their even-mass polonium isotones. ^{199}At has a neutron number of 114. For the polonium data, denoted by closed symbols, see the studies [3,31,32] and references therein. The data for the heavier astatine nuclei are taken from the studies [5,7–10].

The $29/2^+$ isomer and the subsequent states in Band 3 of ^{199}At (see Fig. 4) need a more detailed examination. In the polonium isotone ^{198}Po, an 11^- $\pi(h_{9/2}i_{13/2})$ isomer has been identified at an excitation energy of 2565 keV [38]. The following states have also been identified: 9^- $\nu(f_{5/2}^{-1}i_{13/2}^{-1})$, 8^- $\nu(p_{3/2}^{-1}i_{13/2}^{-1})$, and 7^- $\nu(p_{3/2}^{-1}i_{13/2}^{-1})$. The 11^- isomer populates the 9^- state through an $E2$ transition. The $29/2^+$ isomer in ^{199}At is assumed to originate from the odd proton in the $i_{13/2}$ shell coupled to the maximally aligned $h_{9/2}$ proton pair. However, the subsequent $25/2^+$, $23/2^+$, and $21/2^+$ states can be interpreted as the $J_{\max-1}$ states of the odd $h_{9/2}$ proton coupled to the 9^-, 8^-, and 7^- neutron states of the polonium core just discussed. This major configuration difference between the states results in the $29/2^+$ state becoming isomeric. Figure 12 shows a comparison of the level energies of the yrast $29/2^+$ and $25/2^+$ states with the 11^- and 9^- states of the proposed polonium isotone core. Although the states are not well known throughout the astatine nuclei, a similarity between the curves is clearly visible.

The energy of the $23/2^-$ $\pi(h_{9/2}^2 f_{7/2})$ state increases steadily when approaching the neutron mid-shell (see Fig. 12). However, if the energies of the yrast $29/2^+$ and $25/2^+$ states indeed continue to follow the 11^- and 9^- states, respectively,

TABLE II. The proposed configurations for some of the states in ^{199}At.

	E_{state} (keV)	Configuration
$9/2^-$	0	$\lvert\pi h_{9/2} \otimes {}^{198}\text{Po}_{\,0+}\rangle$
$11/2^-$	655	$\lvert\pi h_{9/2} \otimes {}^{198}\text{Po}_{\,2+}\rangle$
$13/2^-$	600	$\lvert\pi h_{9/2} \otimes {}^{198}\text{Po}_{\,2+}\rangle$
$17/2^-$	1200	$\lvert\pi h_{9/2} \otimes {}^{198}\text{Po}_{\,4+}\rangle$
$21/2^-$	1759	$\lvert\pi h_{9/2} \otimes {}^{198}\text{Po}_{\,6+}\rangle$
$13/2^+$	573	$\lvert(\pi h_{9/2})^2_{0^+} \otimes \pi i_{13/2}\rangle$
$21/2^+$	1943	$\lvert\pi h_{9/2} \otimes {}^{198}\text{Po}_{\,7-}\rangle$
$23/2^+$	2076	$\lvert\pi h_{9/2} \otimes {}^{198}\text{Po}_{\,8-}\rangle$
$25/2^+$	2130	$\lvert\pi h_{9/2} \otimes {}^{198}\text{Po}_{\,9-}\rangle$
$29/2^+$	2293	$\lvert(\pi h_{9/2})^2 \otimes \pi i_{13/2}\rangle_{J_{\max}}$

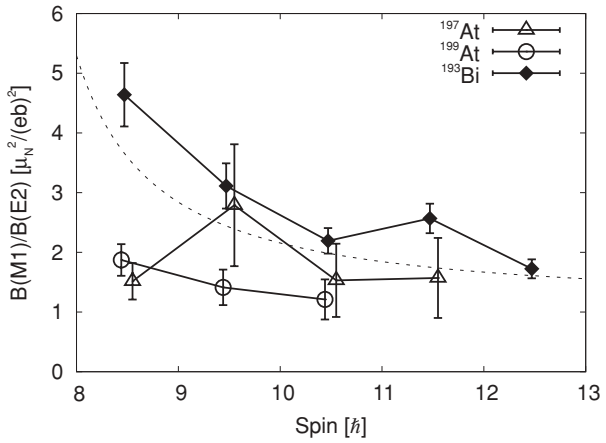

FIG. 10. $B(M1)/B(E2)$ values of the $i_{13/2}$ band in comparison with theory and the corresponding band in ^{193}Bi [33]. The theoretical estimate, denoted by the dashed line, was calculated using the Dönau-Frauendorf model [35,36], assuming $\beta_2 = -0.2$ and $K = 13/2$. The datasets have been shifted slightly along the spin axis for visual purposes.

they are expected to stay rather constant with decreasing neutron number. This results in the $29/2^+$ isomer favoring a feeding to the positive-parity states rather than to the $23/2^-$ state. In ^{205}At, the $29/2^+$ isomer feeds the $23/2^-$ state through an $E3$ transition [10]. However, there is also an $E2$ branch between the $29/2^+$ and $25/2^+$ states in this nucleus. Whereas the single-particle transition strength for this 163-keV $E2$ transition is 0.044 W.u. in ^{199}At, the transition is even more retarded in ^{205}At with a strength of 0.00018 W.u. The $23/2^-$ state is also fed by an $E1$ transition from the $25/2^+$ isomer in the heavier astatine nuclei. The level energy of the $23/2^-$ state, however, rises steadily with decreasing neutron number, making the feeding to it from both the $25/2^+$ and the $29/2^+$ isomer increasingly unfavored.

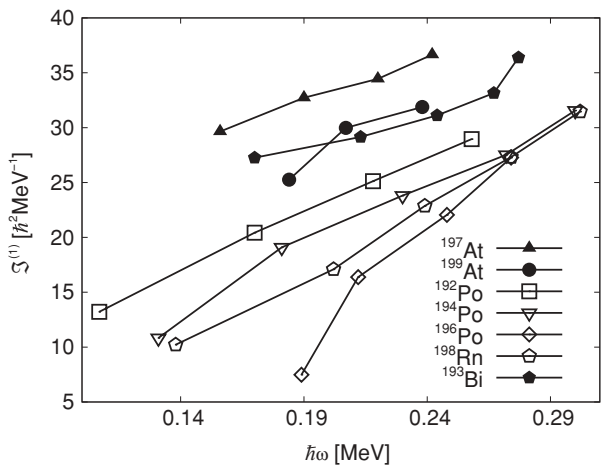

FIG. 11. Experimental kinematic moments of inertia of the rotational band feeding the $13/2^+$ isomer ^{197}At and in ^{199}At in the studied astatine nuclei compared with neighboring oblate deformed nuclei [3,31,33,37]. High-spin data, which exhibit a back bend, have been omitted for ^{193}Bi, for purposes of low-spin comparison.

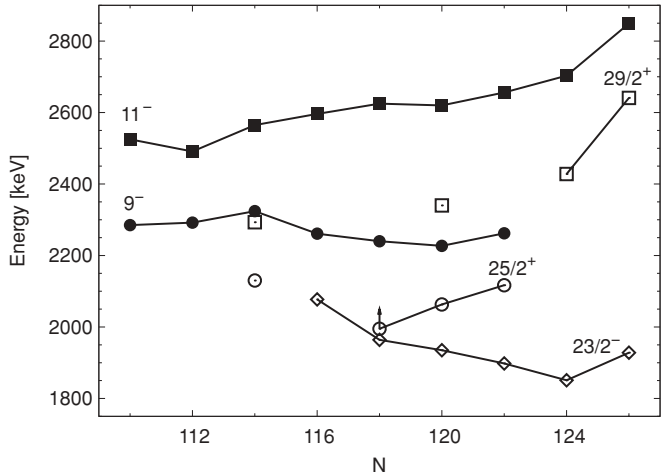

FIG. 12. Level energies of the $29/2^+$, $25/2^+$, and $23/2^-$ states in the odd-mass astatine nuclei, denoted by open symbols, compared with the 11^- and 9^- states in their polonium isotones, denoted by closed symbols. ^{199}At has a neutron number of 114. The data point indicated with an arrow is floating in the level scheme and has been lifted 30 keV in the figure for visual purposes. For the polonium data see the studies [3,31,32] and references therein.

An alternative scheme for the depopulation of the $29/2^+$ isomer is that it decays through the 54-keV $M1$ transition to a $27/2^+$ state, followed by the 133-keV $M1$ and 163-keV $E2$ transitions. This would indicate a strong retardation of 1×10^5 compared to the Weisskopf estimate for the 54-keV $M1$ transition. Similarly hindered $M1$ transitions have been found in the decay of the 10^- $\pi(f_{7/2}i_{13/2})$ isomer in the ^{204,206,208}Rn isotopes [39]. In this case, the subsequent $27/2^+$ and $25/2^+$ states in ^{199}At would be interpreted as the $J_{\max}$ and $J_{\max-1}$ states from the $h_{9/2}$ proton coupled to the 9^- polonium core. A similar pair of states has been reported by Mabala *et al.* in ^{197}Bi [40], which is moreover an isotone to ^{199}At, and by Lönnroth *et al.* [34] in the α-decay daughter ^{195}Bi. In this scheme, the transition between the $25/2^+$ state and the $21/2^+$ state is believed to mimic a core transition between the 9^- and the 7^- states in ^{198}Po. The $25/2^+$ state is reported to be isomeric in the heavier astatine isotopes, with a half-life of some tens of nanoseconds. However, its possible isomeric nature could not be resolved in this study.

V. CONCLUSIONS

The present study clarifies some ambiguities related to the previous results for ^{199}At. We present a strongly coupled rotational band on top of the $13/2^+$ isomer and a series of transitions to the $9/2^-$ ground state. The transitions observed feeding the ground state point to a vibrational structure in ^{199}At. The $11/2^-$ state is above the $13/2^-$ state in energy in ^{199}At, but it drops below the $13/2^-$ state in ^{197}At, as being part of the nonfavored signature partner in the ground-state band. This indicates a strengthening of the coupling between the odd $h_{9/2}/f_{7/2}$ proton and the rotating polonium core. The strongly coupled character of the $i_{13/2}$ band is a sign of collective behavior in both ^{197}At and ^{199}At. The coupling is, however, weaker in ^{199}At, showing a sign of the nucleus

being of transitional nature between spherical structures and the oblate deformed ^{197}At. A $29/2^+$ isomer has been identified to feed the $i_{13/2}$ band through states originated from the odd proton coupled to a neutron pair. The configuration for this isomer is suggested to be $\pi(h^2_{9/2}i_{13/2})$.

ACKNOWLEDGMENTS

This work has been supported through EURONS (European Commission Contract No. RII3-CT-2004-506065) and by the Academy of Finland under the Finnish Centre of Excellence Programme 2006-2011 (Nuclear and Accelerator Based Physics Contract No. 213503). The authors would also like to thank the UK/France (STFC/IN2P3) detector Loan Pool and GAMMAPOOL European Spectroscopy Resource for the loan of the detectors for JUROGAM and GSI for the loan of the VEGA detectors. Support has also been provided by the UK Engineering and Physical Sciences Research Council. U.J. acknowledges support from the Finnish Academy of Science and Letters (the Vilho, Yrjö, and Kalle Väisälä Foundation), P.N. acknowledges support from the Academy of Finland (Contract No. 121110).

[1] K. Heyde, P. Van Isacker, M. Waroquier, J. L. Wood, and R. A. Meyer, Phys. Rep. **102**, 291 (1983).
[2] J. L. Wood, K. Heyde, W. Nazarewicz, M. Huyse, and P. Van Duppen, Phys. Rep. **215**, 101 (1992).
[3] K. Helariutta *et al.*, Eur. Phys. J. A **6**, 289 (1999).
[4] K. Van de Vel *et al.*, Eur. Phys. J. A **17**, 167 (2003).
[5] K. Dybdal, T. Chapuran, D. B. Fossan, W. F. Piel Jr., D. Horn, and E. K. Warburton, Phys. Rev. C **28**, 1171 (1983).
[6] T. P. Sjoreen, D. B. Fossan, U. Garg, A. Neskakis, A. R. Poletti, and E. K. Warburton, Phys. Rev. C **25**, 889 (1982).
[7] T. P. Sjoreen, U. Garg, and D. B. Fossan, Phys. Rev. C **23**, 272 (1981).
[8] T. P. Sjoreen, G. Schatz, S. K. Bhattacherjee, B. A. Brown, D. B. Fossan, and P. M. S. Lesser, Phys. Rev. C **14**, 1023 (1976).
[9] I. Bergström, B. Fant, C. J. Herrlander, K. Wikström, and J. Blomqvist, Phys. Scr. **1**, 243 (1970).
[10] R. F. Davie, A. R. Poletti, G. D. Dracoulis, A. P. Byrne, and C. Fahlander, Nucl. Phys. A **430**, 454 (1984).
[11] K. Andgren *et al.*, Phys. Rev. C **78**, 044328 (2008).
[12] W. Męczyński *et al.*, Eur. Phys. J. A **3**, 311 (1998).
[13] J. Styczeń *et al.*, AIP Conf. Proc. **495**, 255 (1999).
[14] M. Lach *et al.*, Eur. Phys. J. A **9**, 307 (2000).
[15] K. Andgren *et al.*, Phys. Rev. C **77**, 054303 (2008).
[16] C. W. Beausang *et al.*, Nucl. Instrum. Methods Phys. Res. A **313**, 37 (1992).
[17] C. Rossi Alvarez, Nucl. Phys. News **3**, 10 (1993).
[18] M. Leino *et al.*, Nucl. Instrum. Methods Phys. Res. B **99**, 653 (1995).
[19] R. D. Page *et al.*, Nucl. Instrum. Methods Phys. Res. B **204**, 634 (2003).
[20] I. H. Lazarus *et al.*, IEEE Trans. Nucl. Sci. **48**, 567 (2001).
[21] P. J. Nolan, F. A. Beck, and D. B. Fossan, Annu. Rev. Nucl. Part. Sci. **44**, 561 (1994).
[22] E. S. Paul *et al.*, Phys. Rev. C **51**, 78 (1995).
[23] P. Rahkila, Nucl. Instrum. Methods Phys. Res. A **595**, 637 (2008).
[24] D. C. Radford, Nucl. Instrum. Methods Phys. Res. A **361**, 297 (1995).
[25] D. C. Radford, Nucl. Instrum. Methods Phys. Res. A **361**, 306 (1995).
[26] B. Singh, Nucl. Data Sheets **108**, 79 (2007).
[27] H. De Witte *et al.*, Eur. Phys. J. A **23**, 243 (2005).
[28] T. Weckström, B. Fant, T. Lönnroth, V. Rahkonen, A. Källberg, and C.-J. Herrlander, Z. Phys. A **321**, 231 (1985).
[29] F. G. Kondev, Nucl. Data Sheets **108**, 365 (2007).
[30] A. M. Oros, K. Heyde, C. De Coster, B. Decroix, R. Wyss, B. R. Barrett, and P. Navratil, Nucl. Phys. A **645**, 107 (1999).
[31] L. A. Bernstein *et al.*, Phys. Rev. C **52**, 621 (1995).
[32] D. R. Wiseman *et al.*, Eur. Phys. J. A **34**, 275 (2007).
[33] P. Nieminen *et al.*, Phys. Rev. C **69**, 064326 (2004).
[34] T. Lönnroth, C. W. Beausang, D. B. Fossan, L. Hildingsson, W. F. Piel Jr., M. A. Quader, S. Vajda, T. Chapuran, and E. K. Warburton, Phys. Rev. C **33**, 1641 (1986).
[35] F. Dönau and S. Frauendorf, in *Proceedings of the Conference on High Angular Momentum Properties of Nuclei, Oak Ridge, Tennessee, USA, 1982*, edited by N. R. Johnson (Harwood, New York, 1983), p. 143.
[36] F. Dönau, Nucl. Phys. A **471**, 469 (1987).
[37] R. B. E. Taylor *et al.*, Phys. Rev. C **59**, 673 (1999).
[38] M. Lach *et al.*, Z. Phys. A **350**, 207 (1994).
[39] D. Horn, C. Baktash, and C. J. Lister, Phys. Rev. C **24**, 2136 (1981).
[40] G. K. Mabala *et al.*, Eur. Phys. J. A **25**, 49 (2005).